

SCIENTIFIC REPORTS



OPEN

Grassy Silica Nanoribbons and Strong Blue Luminescence

Shengping Wang^{1,*}, Shuang Xie^{2,*}, Guowei Huang¹, Hongxuan Guo³, Yujin Cho⁴, Jun Chen⁴, Daisuke Fujita³ & Mingsheng Xu¹

Received: 17 May 2016

Accepted: 05 September 2016

Published: 26 September 2016

Silicon dioxide (SiO₂) is one of the key materials in many modern technological applications such as in metal oxide semiconductor transistors, photovoltaic solar cells, pollution removal, and biomedicine. We report the accidental discovery of free-standing grassy silica nanoribbons directly grown on SiO₂/Si platform which is commonly used for field-effect transistors fabrication without other precursor. We investigate the formation mechanism of this novel silica nanostructure that has not been previously documented. The silica nanoribbons are flexible and can be manipulated by electron-beam. The silica nanoribbons exhibit strong blue emission at about 467 nm, together with UV and red emissions as investigated by cathodoluminescence technique. The origins of the luminescence are attributed to various defects in the silica nanoribbons; and the intensity change of the blue emission and green emission at about 550 nm is discussed in the frame of the defect density. Our study may lead to rational design of the new silica-based materials for a wide range of applications.

Silicon dioxide (SiO₂) is one of the key materials in many modern technological applications. SiO₂ is the gate dielectric layer that forms the basis of field-effect transistors on the present-day Si integrated circuits¹, and current metal oxide semiconductor (MOS) transistors use SiO₂ films of about 1.3 nm in thickness as the gate dielectric. SiO₂ is also widely explored as an antireflection coating for photovoltaic solar cells². It has been recently demonstrated that a silica layer on top of a silicon absorber significantly reduced the temperature of the underlying absorber under sunlight due to radiative cooling³. In addition, silica-based materials can be worked as catalysts^{4–6} for pollution removal and for biomedical applications⁷.

Owing to the fundamental scientific and technological significance of silica, there is great interest in development of novel structures of silica and understanding the basic structure-property relationships in silica-based materials^{8–15}. It has been found that ultrathin layers of silica on metals occur either as ordered hexagonal structures or as disordered arrangements of non-hexagonal rings. In particular, the crystalline phase of two-dimensional (2D) silica consists of two registered layers of SiO₄ tetrahedra; and the amorphous 2D silica resembles the 2D continuous random network^{8,14,15}. These 2D silica layers can be synthesized in a chemical vapor deposition (CVD) furnace or grown by molecular beam epitaxy on various transition metals, such as Mo, Ru, Pt, Ni, Pd, and Cu^{8,15}. Were the 2D silica layers isolated from metal substrates, like graphene¹⁶ and other 2D layered materials¹⁷, their intrinsic properties and enormous applicability could be investigated at large¹².

Here, we report the accidental discovery of free-standing grassy silica nanoribbons directly grown on SiO₂/Si platform which is commonly used for field-effect transistors fabrication, without providing other precursor. The formation of silica nanoribbons is catalyzed by the co-existence of chromium (Cr) and sulfur (S) in a CVD system. We have performed rigorous analyses of the structure, chemical composition, and cathodoluminescence (CL) properties of the silica nanoribbons. The amorphous silica nanoribbons exhibit strong blue luminescence at about 467 nm. Despite yet unknown technologically relevant performances of the silica nanoribbons as well as 2D silica structures, the understanding of their basic physicochemical properties and controllable growth mechanism may lead to rational design of the new silica-based materials for a wide range of applications.

¹College of Information Science & Electronic Engineering, State Key Laboratory of Silicon Materials, Department of Polymer Science and Engineering, Zhejiang University, Hangzhou 310027, P. R. China. ²State Key Laboratory of Silicon Materials, School of Materials Science and Engineering, Zhejiang University, Hangzhou 310027, P. R. China. ³Nano Characterization Unit, National Institute for Materials Science, 1-2-1 Sengen, Tsukuba 305-0047, Japan. ⁴Nano Electronics Materials Unit, WPI Center for Materials Nanoarchitectonics (MANA), National Institute for Materials Science (NIMS), 1-1 Namiki, Tsukuba, Ibaraki 305-0044, Japan. *These authors contributed equally to this work. Correspondence and requests for materials should be addressed to M.X. (email: msxu@zju.edu.cn)

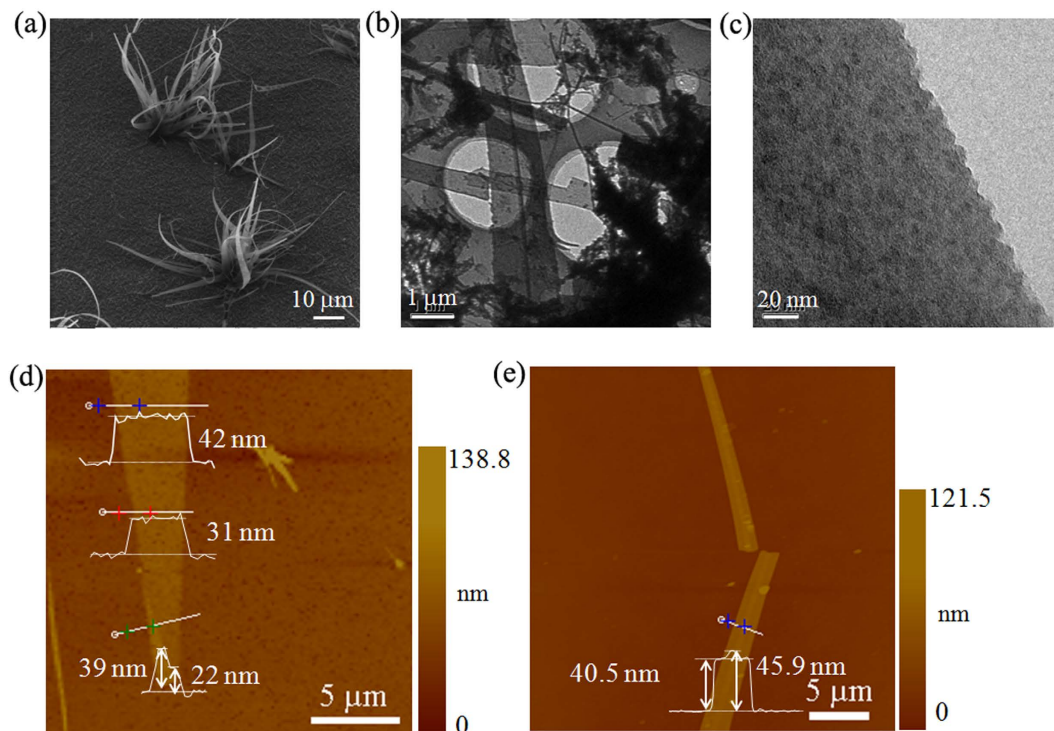


Figure 1. Morphology of silica nanoribbons. (a) Typical SHIM image of bunches of silica nanoribbons. (b,c) TEM images of silica nanoribbons. (d,e) Topographic AFM images and line-profiles showing the thickness of nanoribbons.

Results

Figure 1a shows a representative Helium ion microscopy (HIM)¹⁸ image of the silica nanoribbons grown on SiO₂/Si substrate. The gatherings of nanoribbons with a length of tens of micrometers and varying widths resemble bunches of *chlorophytum comosum* planting into the ground. We further transferred several nanoribbons from the SiO₂/Si substrate onto transmission electron microscope (TEM) Cu meshes to investigate the fine microstructures of the nanoribbons. As displayed in Fig. 1b, the silica nanoribbons are electron-transparent. No ordered structure is observed in the high-resolution TEM image (Fig. 1c and Figure S1 in Supp. Info.), suggesting an amorphous nature of the silica nanoribbons. We had also annealed the nanoribbons for 2 h at 1000. However, amorphous to crystalline structure transition did not occur. The amorphous feature of the nanoribbons is confirmed by the X-ray diffraction (XRD) pattern of the samples (see Figure S2, Supp. Info.). This phenomenon could be attributed to the multilayered structure of the silica nanoribbons, since it has been reported that growing additional layers on top of the crystalline silica monolayer would finally result in amorphous silica films¹⁹. The thickness of individual nanoribbons based on atomic force microscopy (AFM) measurements ranges from 5.4 nm (Fig. 1e) to approximately 50 nm, becoming thinner along the growth direction of the grassy nanoribbons (Fig. 1d,e).

We characterized the chemical composition and Si oxidation states of the silica nanoribbons by employing local scanning Auger electron spectroscopy (AES) technique^{16,20–22}. The Si LVV AES peak position and shape are extremely sensitive to the Si oxidation state²¹. The main peak for elemental Si is centered around 90 eV while that for SiO₂ is located at 76 eV^{21,23}. Figure 2b depicts the AES spectra acquired at different sample locations in Fig. 2a. At the substrate region, i.e., #1 position, the Auger electron signals of both the elemental Si and the Si oxidation states for SiO₂ were detected. By contrast, only the latter was detected on the nanoribbons, i.e., #2 and #3 positions. Figure 2c,e show the Auger electron maps of the Si LVV (Fig. 2d) and O KLL (Fig. 2e), elucidating the chemical distribution of the elements in the silica nanoribbons. Besides, the X-ray photoelectron spectroscopy (XPS) results corroborate the formation of silica nanoribbons (Figure S3, Supp. Info.). Raman spectrum (Figure S4, Supp. Info.) and Fourier transform infrared spectroscopy (FTIR) (Figure S5, Supp. Info.) techniques were also used to analyzed the silica nanoribbons in ambient air.

Discussion

We found the formation of silica nanoribbons when heating very thin Cr films deposited on SiO₂/Si substrates under S atmosphere. However, without either Cr or S, no silica nanoribbon could be obtained. It is a big surprise, to some degree, because a thin Cr layer is normally an adhesive layer of the source/drain electrodes for field-effect transistors on SiO₂/Si platform²⁴. In the literature, the production of monolayer or bilayer 2D silica depended only on the metals and no S was present in their reaction systems^{11–14,25–28}. Therefore, we believed that Cr and S acted as the dual co-catalysts for the growth of silica nanoribbons. Furthermore, on the basis of the morphological observation of the different phases of the growth, the growth mechanism of silica nanoribbons is most likely to be

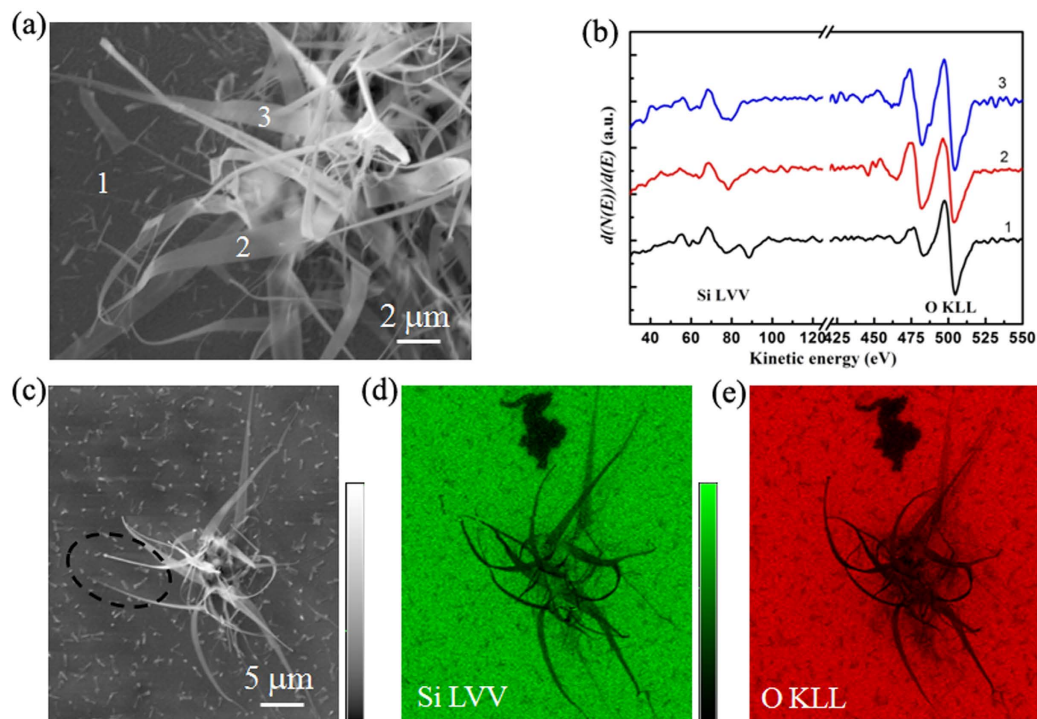


Figure 2. AES characterization of silica nanoribbons. (a) Scanning secondary electron image of the sample, showing the locations of AES spectra acquiring area. (b) Differential AES spectra acquired at positions “1”, “2” and “3” marked in (a). (c) Scanning secondary electron image of the sample, showing the locations of AES mapping. (d) Si LVV Auger electron map acquired in (c). (e) O KLL Auger electron map acquired in (c). The oval in (c) marks movement of the nanoribbon under electron-beam as compared to the positions observed in (d,e).

as follows (see Fig. 3 and Figure S6 in Suppl. Info.). Cracks were firstly generated in the SiO_2 layer on Si with the assistance of Cr and S at high temperature (Fig. 3a); melting of the SiO_2 occurred at the wall of the SiO_2 cracks; and nanoribbons grew *in-situ* at the crack sites. It is also sound from the observations that the Si and O sources for the formation of silica nanoribbons were originated from the melted SiO_2 . The formed silica nanoribbons exhibit various features. Some nanoribbons like a braid (Fig. 3b,c), and some have wedge-shaped edges (Fig. 3d). It is also observed that long silica nanowires with size of about 20 nm (Figure S6e, Suppl. Info.) were produced together with the nanoribbons (see Figs 2c–e and 3). In addition, short silica rods were also produced, lying on the substrate (see Figs 2c–e and 3). The generation of these silica nanostructures on the SiO_2 substrate is rather interesting and the grassy appearance of the silica nanostructures is quite astonishing. The silica nanoribbons are bendable. Moreover, the nanoribbons are sensitive to the exposure of electron beam. As demonstrated in the sequentially acquired AES mappings in Fig. 2c–e, the nanoribbons highlighted in the oval were movable under the electron beam irradiation, which indicates the possibility to manipulate the nanoribbons by electron beam. Also, excessive exposure of electron beam could damage the nanoribbons as observed in Fig. 3b,c. Our grassy silica nanoribbons show distinct morphological characteristics from previous reported silica nanostructures such as nanowires²⁹ and twisted nanobelts and nanosprings³⁰ synthesized by a thermal evaporation method at 1300 °C, porous nanostructures synthesized by complicated solution chemical reactions³¹, and silica nanotubes synthesized by a template-directed method³².

Defects in SiO_2 exert significant influences on its properties such as dielectric performance and luminescence. The defect structure of SiO_2 is extremely sensitive to ionizing radiation^{33,34}. Several kinds of defects in amorphous SiO_2 are optically active and can be studied by luminescence spectroscopy. We investigated the defect-induced luminescence properties of the grassy silica nanoribbons by CL spectroscopy, which is a frequently used technique for high spatial resolution and high-sensitivity detection of defect centers in materials. Figure 4 displays the CL characterization results. All the CL spectra (#2–#9 in Fig. 4a,b) acquired from the different sample locations of nanoribbons possess luminescence features at around 285 nm (4.35 eV, UV band), 467 nm (2.60 eV, blue band), 550 nm (2.25 eV, green band), and 645 nm (1.92 eV, red band)³³. No blue emission can be detected from the substrate (#1). These luminescent bands are common in silica and the specific luminescence centers related to them have been well documented^{35–38}, originating from local atomic rearrangement that deviates from the SiO_4 tetrahedra expected for a perfect silica matrix. The red emission band ascribed to the nonbridging oxygen hole centers (NBOHCs)^{39,40} (see Fig. 4c). The UV emission band can be originated from particular kinds of oxygen vacancy centers (OVCs) such as the disordered Si or neutral oxygen vacancy (Fig. 4c)^{35,37}.

The most striking change in the present set of CL spectra is the luminescent intensity of the blue and green emissions (Fig. 4a,b). At the substrate location (#1), no blue emission appears, in line with previous study on

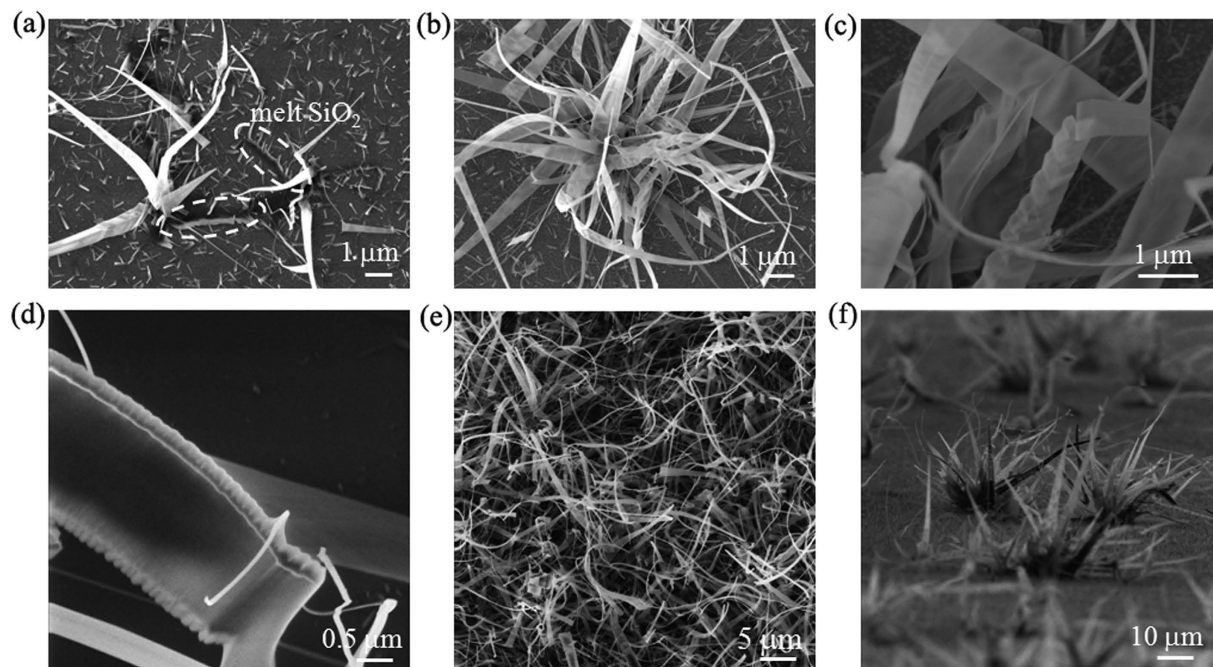


Figure 3. Formation of silica nanoribbons and various fine structures. (a) SEM image showing initial formation of silica nanoribbons at the melted crack-wall sites. (b) SEM image showing a bunch of silica nanoribbons together with nanowires. (c) SEM image showing nanoribbons with different morphologies and deformation of nanoribbons by electron-beam. (d) SHIM image highlighting different edge structures of nanoribbons. (e) SHIM images showing dense nanoribbons. (f) tilt-view of bunched silica nanoribbons.

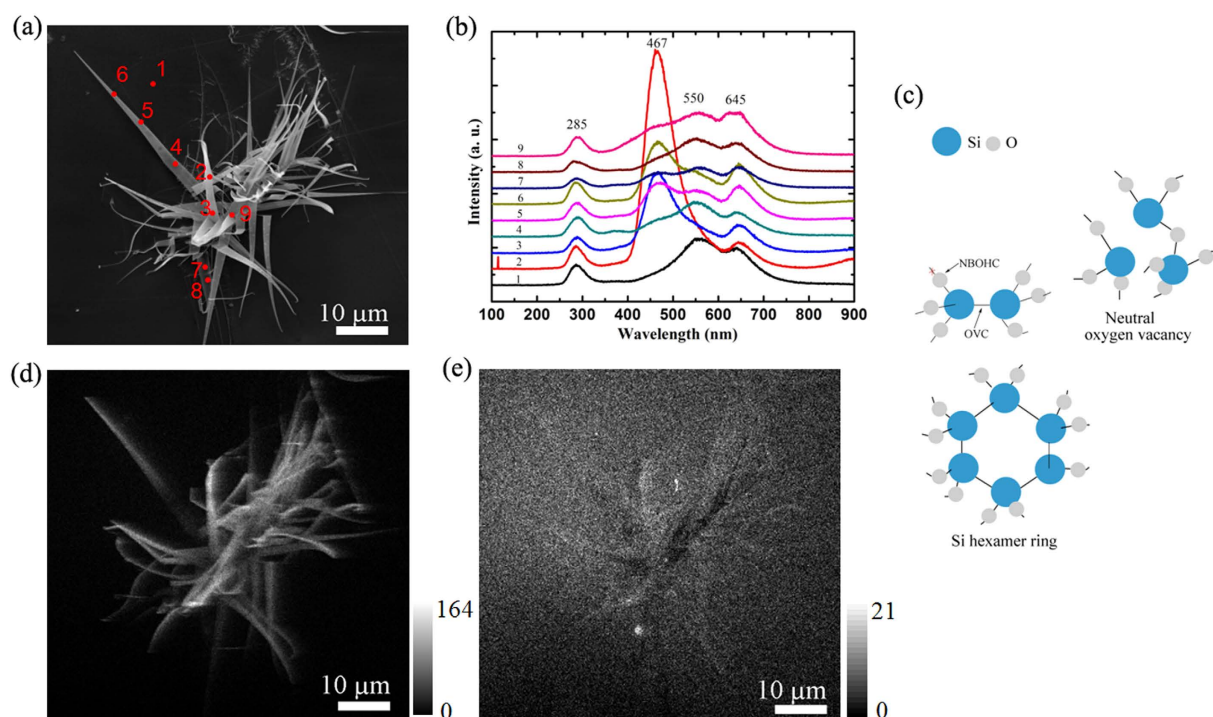


Figure 4. CL characteristics of silica nanoribbons. (a) SEM image showing the positions where the CL spectra were acquired in (b) and emission maps in (e,f). (b) CL spectra acquired at different positions. (c) Schematic illustration of an OVC and a NBOHC, neutral oxygen vacancy, and Si hexamer ring. (d) Blue band map corresponding to (a). (e) Green band map corresponding to (a).

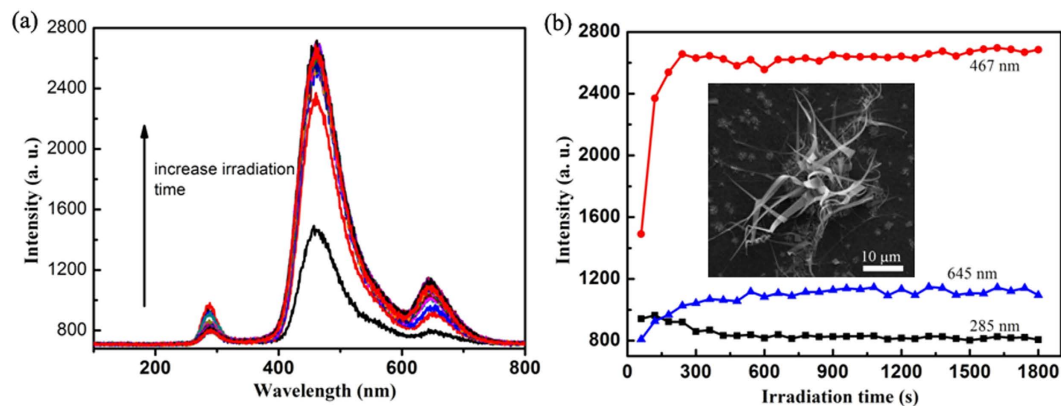


Figure 5. Electron irradiation effect on CL spectrum of silicon nanoribbons. (a) Evolution of CL spectrum with electron irradiation time. (b) Intensity change of UV band, blue band, and red band.

unirradiated amorphous SiO_2 ⁴¹. However, at the apex (#2 as well as #3) of the upright, free-standing silica nanoribbon (Figs 3e and 4a), very strong blue emission is observed. This comparison suggests that the blue emission is most likely to be originated from surface features of the high surface area silica nanoribbons rather than the bulk features of silica. Thus, on the basis of previous study on the blue emission of silica nanostructures^{42–45}, the observed blue emission here could be associated with a defect pair consisting of dioxasilirane ($=\text{Si}(\text{O}_2)$) and a silylene ($=\text{Si}:$). As for the green emission, this may be associated with oxygen-related defects such as silanone ($=\text{Si}=\text{O}$) or dioxasilyrane⁴⁰.

The intensity change of the blue and green emissions is clearly illustrated by the luminescent spectra acquired at the #4, #5 and #6 locations. These phenomena can be explained based on the origins of the luminescence as discussed above. On the one hand, we confirmed the remarkable defective nature of the silica (SiO_x) nanoribbons by TEM-based energy dispersive spectroscopy (EDS) measurements. An atomic ratio ranging from 1.54 to 2.09 between O and Si, typically smaller than 2.0, was obtained for the SiO_x nanoribbons (Figure S7, Supp. Info.). This substoichiometric characteristic suggests the existence of oxygen vacancies in the silica nanoribbons, leading to the strong blue emission. On the other hand, as shown in the AES spectra (Fig. 2b), elemental Si signal was detected at the substrate, which indicates the existence of Si aggregates at the substrate surface resulted from the silica production as addressed above. Therefore, strong green luminescence also appears at the substrate. The intensity mappings of the blue and green emissions are displayed in Fig. 4d,e, respectively. The map of blue emission matches well with the silica nanoribbons (Fig. 4a). The reason resulting in the intensity change of blue and green bands might be the variation of the oxygen content in the silica nanoribbons. Although a quantitative correlation between the oxygen content and the emission intensity is difficult to be concluded at this stage, the lower oxygen content, responsible to the blue emission, could suggest a higher component of silicon aggregates, responsible to the green emission, in the silica nanoribbons. In fact, the OVCs could be described as Si-Si links in the form of dimers, trimers or hexamers^{42,46}. In this perspective, the very weak blue emission at #4 is likely due to the higher content of oxygen than those at #5 and #6 locations.

We investigated the CL properties of a gathering of silica nanoribbons as a function of irradiation time (Fig. 5). The CL emission was excited by continuous irradiation over the observation field with an electron beam of energy 5.0 keV and current 0.1 nA. The very weak green emission of the first collected CL spectrum might be due to the relatively small substrate area because irradiated area is almost fully covered by the silica nanoribbons and silicon aggregates responsible for the emission is not as sensitive to the irradiation as the OVCs. The intensity of the red emission increased with the irradiation time from 0 s to about 600 s; and the UV emission first increased and then decreased within the first 300 s. In the case of the blue emission, the intensity escalated rapidly to a constant intensity within the first 240 s. With irradiation, green emission was being overlapped by the strong blue emission. The trend of the irradiation effect on the luminescence of the nanoribbons is similar to the previous observations on amorphous SiO_2 films⁴¹. Nevertheless, the previous amorphous SiO_2 films⁴¹ did not possess the green emission as detected on our substrate, and we also failed to observe the blue emission from the substrate. The different behaviours of the UV and blue emissions upon the electron irradiation indicate different origins of the emissions. These results indicate that the electron irradiation significantly increases the number of luminescent centers of the silica nanoribbons, strongly dependent on their stoichiometries or absolute deficiency of oxygen atoms over silicon atoms^{47,48}.

In summary, we produced silica nanoribbons by a facile method. The silica nanoribbons look like *chlorophytum comosum*. The silica nanoribbons have a strongly characteristic blue luminescence at about 476 nm as compared to the SiO_2 substrate. Moreover, the silica nanoribbons are flexible and can be manipulated by electron-beam. Whatever the defects responsible for the emissions, this new structure of silica enriches our knowledge of silica-based materials. While the allotropes of bulk silica have made a great impact in fundamental and applied research, the exceptional properties revealed here herald that the grassy silica nanoribbons may present potential applications for, such as composite materials and solar cells as antireflection coating and radiative cooling.

Methods

Silica Nanoribbon Synthesis. We used chemical vapor deposition method to synthesize the silica nanoribbons. SiO₂/Si substrate coated with a thin layer of Cr (99.95%) was used for silica nanoribbon growth under a sulfur atmosphere. Vapor of sulfur was produced by heating sulfur powder. The growth temperature was about 820 °C. We tried to get crystalline silica by annealing the as-prepared silica nanoribbons at 1000 °C for 2 h under Ar atmosphere.

Materials characterization. Characterizations of the silica nanoribbons were carried out by using an atomic force microscope (AFM, Digital Instrument Nanoscope IIIA), a powder X-ray diffractometer (XRD, Rigaku D/Max Ultima IV), a field emission scanning electron microscope (FESEM, Hitachi S-4800), a transmission electron microscope (TEM, FEI TECNAIG2 F20-TWIN) equipped with an energy dispersive X-ray spectroscope (EDS), and X-ray photoelectron spectroscopy (ESCALAB 250Xi system). The topographic images of the silica nanoribbons were acquired in the tapping mode. The SEM images were obtained on a Hitachi S4800 field-emission SEM system with an accelerating voltage of 3.0 kV. The XRD was operated at 40 kV, 40 mA for Cu K α radiation ($\lambda = 1.5418 \text{ \AA}$). XPS was performed using Al K α as the source and the C 1s peak at 284.8 eV as an internal standard. An acceleration voltage of 200 kV was used for EDS measurement. Raman spectrum was obtained by using Renishaw inVia system with a 532 nm laser in ambient air. Fourier transform infrared spectroscopy (FTIR) was recorded on a Bruker Vector 22 spectrofluorometer in ambient air.

Cathodoluminescence (CL) Characterization. CL measurement was performed by using field emission scanning electron microscope (FESEM; HITACHI SU6600) equipped with CL system (HORIBA MP32). An acceleration voltage of 5.0 kV and beam current of 0.1 nA were used for CL measurement.

Scanning Auger Electron Spectroscopy. The AES measurements were performed at room temperature with a scanning Auger electron spectroscope (ULVAC-PHI model SAM650) with a cylindrical mirror analyzer. The takeoff angle of the instrument was 42°. AES spectra were acquired with a primary electron beam of 10 keV. The incident electron beam current for the AES spectra was about 2.0 nA, as calibrated with a Faraday cup before and after each measurement. Area-analysis mode can be chosen to acquire electron spectra. Acquiring of each elemental map (512 \times 512 pixels) took \sim 3.5 h.

References

- Muller, D. A. *et al.* The electronic structure at the atomic scale of ultrathin gate oxides. *Nature* **399**, 758–761 (1999).
- Peng, K. Q. & Lee, S. T. Silicon nanowires for photovoltaic solar energy conversion. *Adv. Mater.* **23**, 198–215 (2011).
- Zhu, L. X., Ramanab, A. P. & Fan, S. H. Radiative cooling of solar absorbers using a visibly transparent photonic crystal thermal blackbody. *Proc. Natl. Acad. Sci. USA* **112**, 12282–12287 (2015).
- Liu, J. H., Wei, X. F., Wang, X. & Liu, X. W. High-yield synthesis of ultrathin silica-based nanosheets and their superior catalytic activity in H₂O₂ decomposition. *Chem. Commun.* **47**, 6135–6137 (2011).
- Sun, M. *et al.* Methane reacts with heteropolyacids chemisorbed on silica to produce acetic acid under soft conditions. *J. Am. Chem. Soc.* **135**, 804–810 (2013).
- Dinker, M. K. & Kulkarni, P. S. Recent advances in silica-based materials for the removal of hexavalent chromium: a review. *J. Chem. Eng. Data* **60**, 2521–2540 (2015).
- Tang, F. Q., Li, L. L. & Chen, D. Mesoporous silica nanoparticles: synthesis, biocompatibility and drug delivery. *Adv. Mater.* **24**, 1504–1534 (2012).
- Shaikhutdinov, S. & Freund, H. J. Ultrathin silica films on metals: the long and winding road to understanding the atomic structure. *Adv. Mater.* **25**, 49–67 (2013).
- Schroeder, T., Giorgi, J. B., Bäumer, M. & Freund, H. J. Morphological and electronic properties of ultrathin crystalline silica epilayers on a Mo(112) substrate. *Phys. Rev. B* **66**, 165422 (2002).
- Löffler, D. *et al.* Growth and structure of crystalline silica sheet on Ru(0001). *Phys. Rev. Lett.* **105**, 146104 (2010).
- Lichtenstein, L., Heyde, M. & Freund, H. J. Crystalline-vitreous interface in two dimensional silica. *Phys. Rev. Lett.* **109**, 106101 (2012).
- Huang, P. Y. *et al.* Direct imaging of a two-dimensional silica glass on graphene. *Nano Lett.* **12**, 1081–1086 (2012).
- Romdhane, F. B. *et al.* *In situ* growth of cellular two-dimensional silicon oxide on metal substrates. *ACS Nano* **7**, 5175–5180 (2013).
- Huang, P. Y. *et al.* Imaging atomic rearrangements in two-dimensional silica glass: watching silica's dance. *Science* **342**, 224–227 (2013).
- Shaikhutdinov, S. & Freund, H. J. Ultra-thin silicate films on metals. *J. Phys.: Condens. Matter* **27**, 443001 (2015).
- Liang, T. *et al.* Graphene nucleation preferentially at oxygen-rich Cu sites rather than on pure Cu surface. *Adv. Mater.* **27**, 6404–6410 (2015).
- Xu, M. S., Liang, T., Shi, M. M. & Chen, H. Z. Graphene-like two-dimensional materials. *Chem. Rev.* **113**, 3766–3798 (2013).
- Guo, H. X., Gao, J. H., Ishida, N., Xu, M. S. & Fujita, D. Characterization of two-dimensional hexagonal boron nitride using scanning electron and scanning helium ion microscopy. *Appl. Phys. Lett.* **104**, 031607 (2014).
- Stacchiola, D. J. *et al.* Growth of stoichiometric subnanometer silica films. *Appl. Phys. Lett.* **92**, 011911 (2008).
- Xu, M. S., Fujita, D., Gao, J. H. & Hanagata, N. Auger electron spectroscopy: a rational method for determining. *ACS Nano* **4**, 2937–2945 (2010).
- Xu, M. S., Fujita, D. S. & Hanagata, N. Monitoring electron-beam irradiation effects on graphenes by temporal Auger electron spectroscopy. *Nanotechnology* **21**, 265705 (2010).
- Xu, M. S., Fujita, D., Sagisaka, K., Watanabe, E. & Hanagata, N. Production of extended single-layer graphene. *ACS Nano* **5**, 1522–1528 (2011).
- Chao, S. S. *et al.* A study of chemical bonding in suboxides of silicon using Auger electron spectroscopy. *J. Vac. Sci. Technol. A* **4**, 1574–1579 (1986).
- Xu, M. S., Nakamura, M., Sakai, M. & Kudo, K. High-performance bottom-contact organic thin-film transistors with controlled molecule-crystal/electrode interface. *Adv. Mater.* **19**, 371–372 (2007).
- Weissenrieder, J. *et al.* Atomic structure of a thin silica film on a Mo(112) substrate: a two-dimensional network of SiO₄ tetrahedra. *Phys. Rev. Lett.* **95**, 076103 (2005).
- Lichtenstein, L., Büchner, C. & Yang, B. The atomic structure of a metal-supported vitreous thin silica film. *Angew. Chem. Int. Ed.* **51**, 404–407 (2012).

27. Altman, E. I., Götzen, J., Samudrala, N. & Schwarz, U. D. Growth and characterization of crystalline silica films on Pd(100). *J. Phys. Chem. C* **117**, 26144–26155 (2013).
28. Romdhane, F. B., Björkman, T., Krashennikov, A. V. & Banhart, F. Solid-state growth of one- and two-dimensional silica structures on metal surfaces. *J. Phys. Chem. C* **118**, 21001–21004 (2014).
29. Shang, N. G. *et al.* Luminescence centres in silica nanowires. *Nanotechnology* **17**, 3215–3218 (2006).
30. Zhang, Z. Y. *et al.* Synthesis, growth mechanism, and light-emission properties of twisted SiO₂ nanobelts and nanosprings. *J. Chem. Phys.* **129**, 164702 (2008).
31. Li, Y. *et al.* Preparation of chiral mesoporous silica nanotubes and nanoribbons using a dual-templating approach. *Chem. Mater.* **25**, 307–312 (2013).
32. Zhang, W. J., Hong, C. Y. & Pan, C. Y. Fabrication and characterization of silica nanotubes with controlled dimensions. *J. Mater. Chem. A* **2**, 7819–7828 (2014).
33. Koyama, H. Cathodoluminescence study of SiO₂. *J. Appl. Phys.* **51**, 2228 (1980).
34. Kalceff, M. A. S. & Phillips, M. R. Cathodoluminescence microcharacterization of the defect structure of quartz. *Phys. Rev. B* **52**, 3122 (1995).
35. Skuja, L. Optically active oxygen-deficiency-related centers in amorphous silicon dioxide. *J. Non-Cryst. Solids* **239**, 16–48 (1998).
36. Salh, R., Czarnowski, A. V. & Fitting, H. Cathodoluminescence of non-stoichiometric silica: the role of oxygen. *J. Non-Cryst. Solids* **353**, 546–549 (2007).
37. Cuff, S. *et al.* Investigation of emitting centers in SiO₂ codoped with silicon nanoclusters and Er³⁺ ions by cathodoluminescence technique. *J. Appl. Phys.* **108**, 113504 (2010).
38. Fukushima, Y., Chanthaphan, A., Hosoi, T., Shimura, T. & Watanabe, H. Cathodoluminescence study of radiative interface defects in thermally grown SiO₂/4H-SiC(0001) structures. *Appl. Phys. Lett.* **106**, 261604 (2015).
39. Vaccaro, L., Cannas, M., Radzig, V. & Boscaino, R. Luminescence of the surface nonbridging oxygen hole center in silica: Spectral and decay properties. *Phys. Rev. B* **78**, 075421 (2008).
40. Vaccaro, L., Morana, A., Radzig, V. & Cannas, M. Bright visible luminescence in silica nanoparticles. *J. Phys. Chem. C* **115**, 19476–19481 (2011).
41. Goldberga, M., Fitting, H. J. & Trukhin, A. Cathodoluminescence and cathodoelectroluminescence of amorphous SiO₂ films. *J. Non-Cryst. Solids* **220**, 69–77 (1997).
42. Uchino, T., Kurumoto, N. & Sagawa, N. Structure and formation mechanism of blue-light-emitting centers in silicon and silica-based nanostructured materials. *Phys. Rev. B* **73**, 233203 (2006).
43. Anjiki, A. & Uchino, T. Visible photoluminescence from photoinduced molecular species in nanometer-sized oxides: crystalline Al₂O₃ and amorphous SiO₂ nanoparticles. *J. Phys. Chem. C* **116**, 15747–15755 (2012).
44. Spallino, L. *et al.* Visible-ultraviolet vibronic emission of silica nanoparticles. *Phys. Chem. Chem. Phys.* **16**, 22028–22034 (2014).
45. Davies, G. L., McCarthy, J. E., Rakovich, A. & Gun'ko, Y. K. Towards white luminophores: developing luminescent silica on the nanoscale. *J. Mater. Chem.* **22**, 7358–7365 (2012).
46. Salh, R., Czarnowski, A. V., Zamoryanskaya, M. V., Kolesnikova, E. V. & Fitting, H. Cathodoluminescence of SiO_x under-stoichiometric silica layers. *J. Phys. Status Solidi A* **203**, 2049–2057 (2006).
47. Nishikawa, H., Tohmon, R., Ohki, Y., Nagasawa, K. & Hama, Y. Defects and optical absorption bands induced by surplus oxygen in high-purity synthetic silica. *J. Appl. Phys.* **65**, 4672 (1989).
48. Nishikawa, H. *et al.* Generation mechanism of photoinduced paramagnetic centers from preexisting precursors in high-purity silicas. *Phys. Rev. B* **41**, 7828 (1990).

Acknowledgements

This work was supported by the Program for New Century Excellent Talents in University (NCET-12-0494), the Research Fund for the Doctoral Program of Higher Education (20130101110123), the Program for 14th China-Japan S&T Cooperation (2013DFG52800), and by the National Natural Science Foundation of China (Grants 51472219). We thank Material Analysis Station at National Institute for Materials Science (NIMS), Japan for assistance of AES measurement.

Author Contributions

M.X. conceived the study and performed the AES study with assistance of D.F. Experiments were conducted by S.W., S.X., G.H., H.G., Y.C., J.C. and M.X. wrote the paper and all authors discussed the results and commented on the manuscript.

Additional Information

Supplementary information accompanies this paper at <http://www.nature.com/srep>

Competing financial interests: The authors declare no competing financial interests.

How to cite this article: Wang, S. *et al.* Grassy Silica Nanoribbons and Strong Blue Luminescence. *Sci. Rep.* **6**, 34231; doi: 10.1038/srep34231 (2016).



This work is licensed under a Creative Commons Attribution 4.0 International License. The images or other third party material in this article are included in the article's Creative Commons license, unless indicated otherwise in the credit line; if the material is not included under the Creative Commons license, users will need to obtain permission from the license holder to reproduce the material. To view a copy of this license, visit <http://creativecommons.org/licenses/by/4.0/>

© The Author(s) 2016